Four-dimensional coronary morphology and computational hemodynamics

Andreas Wahle,[a] Steven C. Mitchell,[a] Sharan D. Ramaswamy,[b]
Krishnan B. Chandran,[b] and Milan Sonka[a]

The University of Iowa, [a]Department of Electrical and Computer Engineering,
and [b]Department of Biomedical Engineering, Iowa City, IA 52242–1527, USA

ABSTRACT

Conventional reconstructions from intravascular ultrasound (IVUS) stack the frames as acquired during the pullback of the catheter to form a straight three-dimensional volume, thus neglecting the vessel curvature and merging images from different heart phases. We are developing a comprehensive system for fusion of the IVUS data with the pullback path as determined from x-ray angiography, to create a geometrically accurate 4-D (3-D plus time) model of the coronary vasculature as basis for computational hemodynamics. The overall goal of our work is to correlate shear stress with plaque thickness. The IVUS data are obtained in a single pullback using an automated pullback device; the frames are afterwards assigned to their respective heart phases based upon the ECG signal. A set of 3-D models is reconstructed by fusion of IVUS and angiographic data corresponding to the same ECG-gated heart phase; methods of computational fluid dynamics (CFD) are applied to obtain important hemodynamic data. Combining these models yields the final 4-D reconstruction. Visualization is performed using the platform-independent VRML standard for a user-friendly manipulation of the scene. An extension for virtual angioscopy allows an easy assessment of the vessel features within their local context. Validation was successfully performed both in-vitro and in-vivo.

Keywords: Coronary Atherosclerosis, Computational Hemodynamics, 4-D Reconstruction, Data Fusion, Intravascular Ultrasound, X-ray Angiography

1. INTRODUCTION

Cardiovascular diseases are major causes of human death.[1] Therefore, the study of the progression of disease as a function of hemodynamics in human vasculature has gained recent interest. Since the cardiovascular system is a site of frequent initiation and growth of atherosclerotic lesions, a number of experimental and computational simulation studies has been reported on the fluid mechanics in arteries.[2–5] Previous studies of computational hemodynamics have implicated regions of flow reversal and separation, as well as relatively low wall shear stresses and oscillating shear stresses, as causes for initiation and growth of atherosclerotic plaques. Specific areas of disease tend to be concentrated proximally in all major coronary branches with an asymmetric distribution around each respective circumference.[6] While these observations point directly to fluid mechanic implications towards atheroma evolution, it remains that the hypothesis of geometrical implications on shear stress variations within the coronary arteries has yet to be effectively tested. In particular, since the added constraint on the coronaries is that of time-dependent movement of vessel curvature, torsion, rotation, wall diameter, and length,[7] in totality the hemodynamic implications in the coronary vessels, taking the geometrical changes into account is highly complex.

X-ray angiography and intravascular ultrasound (IVUS) represent the most commonly used diagnostic tools to assess cardiovascular diseases. Selective coronary angiography provides projectional x-ray images of contrast-filled coronary vessels and has been clinically used for decades. Several semi-automated tools are available for evaluation of local stenoses.[8–10] While angiography provides detailed images of the vessel lumen, it offers no information about the extent and the composition of the plaque covering the inner coronary wall. Intravascular ultrasound of the coronary arteries has become a well-established method complementary to angiography. The vessel cross-sections can be imaged by inserting an ultrasonic transducer directly into the vessel lumen. In this way, the lumen as well as the vessel wall are depicted accurately, including information about the composition and location of the plaque.[10–12] A major drawback of IVUS is its inability to consider the vessel curvature and the orientation of the imaging catheter

E-mail: <andreas-wahle@uiowa.edu>; http://www.engineering.uiowa.edu/~awahle; Fax: +1-319-335-6028

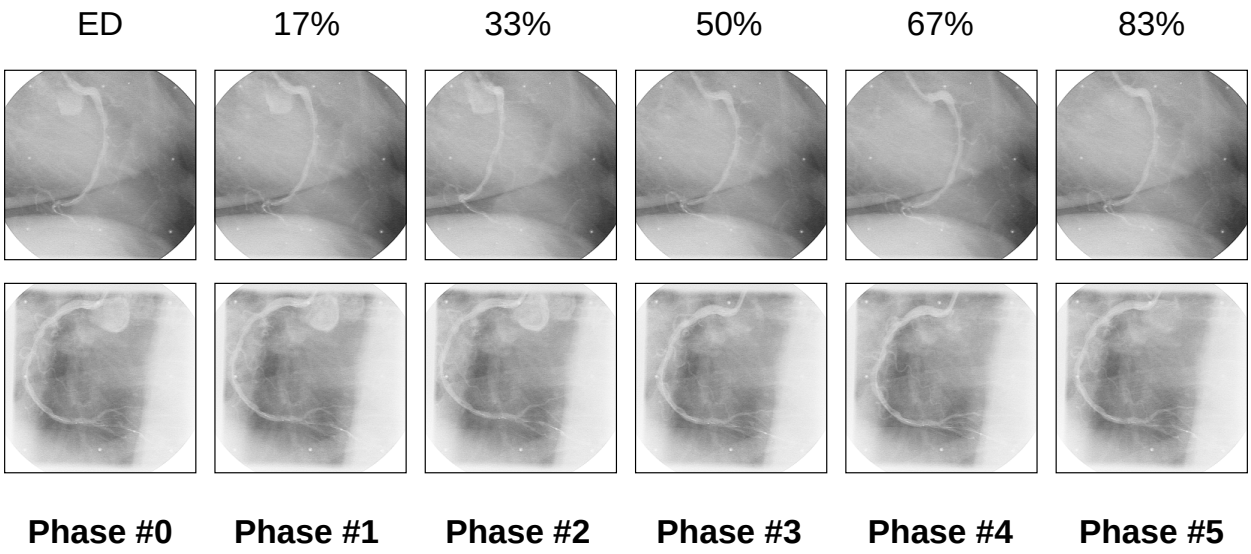

Figure 1. The six biplane angiographic pairs of the heart cycle selected for fusion, with percentages within the R–R interval; upper row: plane A (75° RAO), lower row: plane B (20° LAO).

when assigning the detected plaque to specific locations. Therefore, we have developed a fusion system that combines the geometrical data obtained from biplane angiography with the cross-sectional data delivered by IVUS.[13–16]

To consider the true flow within the diseased moving artery, methods of computational fluid dynamics (CFD) are applied on the 3-D and 4-D models of the vessel, as generated by the fusion system. Utilizing CFD is pivotal in understanding how time-dependence of the vessel geometry parameters effect the blood flow parameters. It is expected to be the best feasible method to predict the significance of geometry related factors to plaque formation. Therefore, the 3-D model resulting from the fusion process needs to be extended into 4-D (specifically, 3-D plus time, where *time* relates to any given heart phase). The raw image data from angiography and IVUS can be split into n sets of different heart phases $[0 \cdots n-1]$, where the ECG signal is used to assign each angiogram or frame to its respective heart phase.

Aside from quantitative analysis, visualization is an important aspect to allow effective access to the reconstructed and analyzed data. For a platform-independent visualization, a standardized description language is utilized, the Virtual Reality Modeling Language (VRML).[17] It a allows the representation of both 3-D and animated 4-D surface-oriented models.[16] The interaction can be substantially complex; an example is the virtual angioscopy approach presented in a companion paper to a parallel conference.[18]

This paper presents a work in progress report on the three- and four-dimensional CFD analysis on human arteries. We will show how the 4-D model is extracted from the two modalities, as extension of the 3-D fusion approach reported earlier,[13–16] a process in which we have achieved already a high accuracy. We further report a CFD feasibility study in 3-D — yet to be extended to 4-D — on a human artery in end-diastolic phase, along with a comprehensive validation in a well-established uniform tube model.

2. METHODS

The overall process can be split into the following components:

1. Acquire IVUS and angiographic data and sort them by the heart phase;
2. segment IVUS and angiographic data for the lumen and other features;
3. determine the 3-D location for each point of the vessel lumen in each considered heart phase;
4. perform CFD analyses in each heart phase, where movement patterns will have to be considered in 4-D;
5. use the reconstructed 3-D or 4-D data for visualization and/or further quantification.

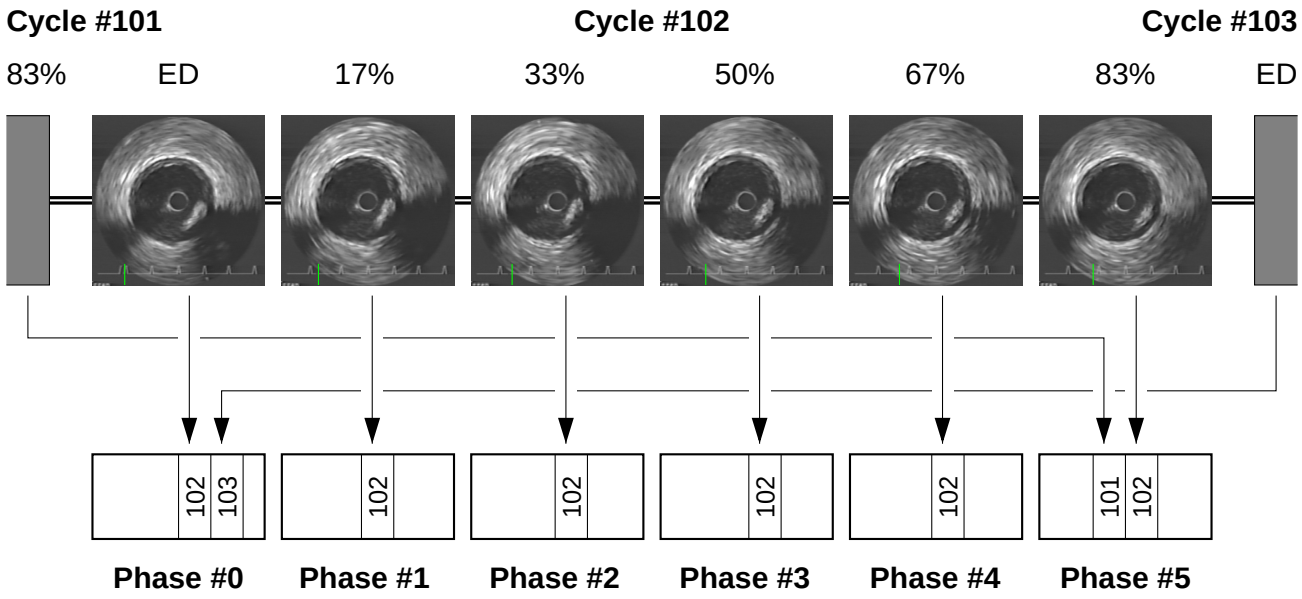

Figure 2. Process of assigning the IVUS frames to their respective heart phase.

2.1. Data acquisition

IVUS and angiographic data are acquired independently from each other. For the 4-D case in-vivo, separate sets of IVUS frames and corresponding angiographic images are acquired for each heart phase according to the ECG signal. As a reference, the *R*-wave is used to identify the end-diastolic phase. Specific percentiles are then used between adjacent *R*-waves to determine the intermediate phases. While only a single cycle is considered in the angiographic images, the IVUS frames have to be merged from different heart cycles due to continuing heart activity during the pullback.[19] Therefore, frames representing the same heart phase are collected as sets in an interlaced way. An example of the acquisition scheme with n=6 phases is shown in Figures 1 and 2.

2.1.1. Intravascular ultrasound

The fusion system is based on the sheathed design of mechanically driven catheters[10] currently using a fixed frequency of 30–40 MHz at a diameter between 2.9F and 3.2F (a *French* corresponds to $\frac{1}{3}$mm). The IVUS catheter delivers an image which represents the vessel cross section at the current location only. ECG data is usually provided as overlay in the images. Motorized continuous pullback ensures that a specific vessel segment is covered, and that the location can be approximated from the time passed since the pullback started. The sheathed design has the major advantage of providing a stable pullback path, since only the core is moving in the direction of the pullback and the sheath remains in its position. During the following fusion process, the catheter path is predicted from a single angiographic pair of the same heart phase taken at the start of the pullback.[14–16]

2.1.2. Biplane angiography

The biplane angiograms are taken immediately at the start of the pullback and cover at least one heart cycle. They are used to extract the catheter path automatically along the expected pullback trajectory, and to find the vessel lumen outline as a reference for the following fusion process. State of the art is digital storage of the angiograms in the DICOM format on Recordable Compact Discs (CD–R),[10] for which we have developed a biplane DICOM viewer that allows fully-synchronous navigation within both planes. The digital format has the major advantage that the parameters of the selected imaging geometry, used as basis for the angiographic 3-D reconstruction,[20] as well as the ECG curves, are available along with their corresponding image data. Before used for reconstruction, the angiograms are dewarped for geometric distortions.[10]

2.2. Segmentation

For the segmentation of the IVUS images as well as the angiograms, dynamic programming methods are utilized.[16,21] While the 3-D models are generated separately for all heart phases, some information is passed between the phases

for the IVUS segmentation as outlined in Section 2.4. Segmentation of the IVUS data includes a longitudinal pre-segmentation to obtain the regions of interest for the cross-sectional directions; in the angiograms, the user specifies roughly the catheter path, where both the catheter and the lumen outline are then extracted automatically within a region of interest formed by a cubic spline.[16]

2.3. Fusion

Fusion includes a per-phase mapping of the segmented IVUS data from 2-D into 3-D space, based upon the pullback path during acquisition. Therefore, the movement pattern of the catheter during the pullback has to be determined as accurately as possible. The problem of assigning the IVUS data into 3-D space is actually two-fold:

1. The IVUS frames have to be related to 3-D locations, and
2. their orientations have to be determined.

2.3.1. Frame location

Based upon the stable pullback behavior of the sheathed catheter design, the location of any IVUS frame with known acquisition time can be determined by figuring the time passed from the start of the pullback until this specific frame was taken. Using the reconstructed catheter path, the segment previously visited by the transducer can be easily measured, and thus the location reached after imaging this previous vessel segment can be established. It is important to remember that this is done for each heart phase separately, assuming that the catheter reaches approximately the same location again from heart beat to heart beat. The three-dimensional reconstruction of the catheter path (along with the angiographic lumen outline) is performed using a well-established and validated method developed at the German Heart Institute of Berlin.[20]

2.3.2. Frame orientation

The complex process of determining the 3-D orientation of each IVUS frame has been described in detail before.[13–15] Our two-step approach combines the analytical determination of the *relative* changes in orientation between adjacent IVUS frames based upon the Frenet–Serret formulas with a non-iterative statistical approach to obtain the *absolute* orientation of the frame set in 3-D from the initial orientation. The catheter within the vessel lumen is used as reliable landmark for the overall optimum match of the frame set, utilizing the out-of-center position of the imaging catheter relative to the lumen. After mapping the IVUS data and all related contour information into their respective 3-D locations within the geometrically correct oriented frames, the 3-D data set for the specific heart phase is finalized.

2.4. Reconstruction and fusion of 4-D data sets

In general, the 4-D data set is created from the complete set of 3-D models. However, there are certain assumptions that can be made when reconstructing the same object over time that benefit the process. The segmentation of the IVUS frames is done phase by phase; after all the regions of interests have been derived from one phase, they can be used as initial guess for the next phase, whose frames are basically next to the ones segmented before. Thus, only slight adjustments may be necessary, and the overall process of IVUS segmentation may be reduced substantially.

A further aspect where the close relation between the phases benefits the process is the determination of the absolute orientation. It can be assumed safely that from phase to phase, only slight rotations of the overall frame set should occur; therefore, the parameters of the absolute orientation analysis over all phases can be utilized to tie the phases with each other. Since the initial orientation is derived from a reference plane determined by bilinear regression from the catheter path,[14,15] the initial orientations and therefore all correction angles are connected. This results in a more stable statistical basis for determination of the correction angle.

2.5. Downsampling and smoothing of the reconstructed 3-D/4-D data

The data has to be downsampled and smoothed substantially to be suitable for computational hemodynamics and visualization. The IVUS segmentation results in a set of 720 vertex points per contour, each of which corresponding to a 0.5° radial sector relative to the catheter. The centroid of the contour is determined, and then a set of representative vertex points in larger sectors determined. For each radial sector, all vertex points from IVUS segmentation located within this sector are resampled into a polar coordinate system, and then the representative vertex point determined by calculating the averages of polar angle and distance to the centroid. Note that the number of vertex points within each sector differs, since the catheter is not necessarily located in the vessel center.

In longitudinal direction, no downsampling takes place, since the number of frames is limited. However, if performance issues require a downsampling, the representative vertex points in the same radial sector can be combined over multiple frames. Smoothing is usually necessary to compensate for remaining artifacts from acquisition, ECG gating, and segmentation. Either averaging or 3-D spline-based smoothing functions are available. Also, a method for non-shrinking smoothing of contours in 3-D was developed.[22]

Along the time-axis, neither smoothing nor down-sampling are performed. Except for the two cases outlined in the previous subsection, the 3-D models are processed separately from each other and then combined to form the 4-D model.

2.6. Computational hemodynamics

CFD analysis is employed in order to delineate the flow-induced stresses and their relationship with development and growth of atherosclerosis. The coronary arteries have a complex curved geometry with distensible vessel walls. Furthermore, the arteries have to follow the translational and rotational movements of the heart over the cardiac cycle. For the CFD simulation of flow through the coronary vessels, we employ a finite-volume CFD code developed at the University of Iowa (U2RANS).* This code has the capability of simulating steady and unsteady laminar and turbulent flows. Furthermore, the code allows specification of moving boundaries as well as pre-specified motion of the arteries and hence is ideally suited to simulate the fluid mechanics in the coronary vessels.

The input grid for this system was created using a commercial grid generation software (GRIDGEN).† So far, only structured grids have been used for CFD analysis, i.e., the dimensions are the same over the entire object to be analyzed. The methodology of developing a 3-D grid requires to convert the tube-like segment into a closed surface. Next, this surface is split and meshed into six independent domains that make up one volumetric or 3-D mesh suitable as input for the CFD analysis. The grid size is defined by three dimensions i, j, k. While j is the number of cross-sections, i and k refer to the cross-sectional distribution of the grid points. The six surfaces result from the first [0] and last $[j-1]$ cross-sections, and in analogy, the remaining four surfaces are defined in i-dimension $[0, i-1]$ and k-dimension $[0, k-1]$. Typical size of the grid used in this study is 15,000 points ($i \times j \times k = 10 \times 150 \times 10$).

After generating the grid and prescribing all initial values (inlet velocities, pressure, etc.), an iterative procedure is employed by the CFD software to solve the space conservation, continuity and momentum equations, assuming a known pressure, and then solving the pressure-correction equation to satisfy the continuity equation.

2.7. Visualization of the 3-D/4-D data

Visualization is performed using the VRML language,[17] which is an ISO standard. The VRML code is generated automatically from the frame, contour, and CFD data. It can be visualized using public-domain VRML viewers, such as the CosmoPlayer 2.1‡ plug-in for Netscape 4.7x or MS Internet-Explorer.

2.7.1. 3-D model of a single heart phase

The fact that the segmentation and fusion process for the IVUS data results in contours with a fixed number of vertices perpendicular to the catheter path simplifies the triangulation of the data as compared to tomographic data from CT or MR. Facets between adjacent contours are created by a fixed zig-zag pattern, and then combined to an `IndexedFaceSet` structure in VRML. One 3-D indexed face set is created for each heart phase, which can be visualized independently.

2.7.2. Animation of the full heart cycle

VRML provides `TimeSensor` and `CoordinateInterpolator` nodes to control the animation of 3-D objects. As a given restriction, all heart phases are expected to be represented in 3-D models of equal size, i.e., with the same number of vertex points per contour as well as the same number of contours. A single `IndexedFaceSet` VRML node is used to model the raw object, while a `CoordinateInterpolator` is responsible to animate the vertices of the `IndexedFaceSet` node. The contours are therefore no longer kept in the `IndexedFaceSet` itself, but rather as interlaced lists in the `CoordinateInterpolator` node. A similar strategy can be found in literature as well.[17] The result is a smooth linearly interpolated movement of the modeled vessel segment. Further controls may be added to improve interaction, similar to those shown in the virtual angioscopy realization.[18]

*U2RANS was developed by Yong G. Lai, Iowa Institute of Hydraulic Research at The University of Iowa

†Pointwise Inc., Fort Worth TX, USA

‡Cosmo Software, Computer Associates International Inc., Islandia NY, USA

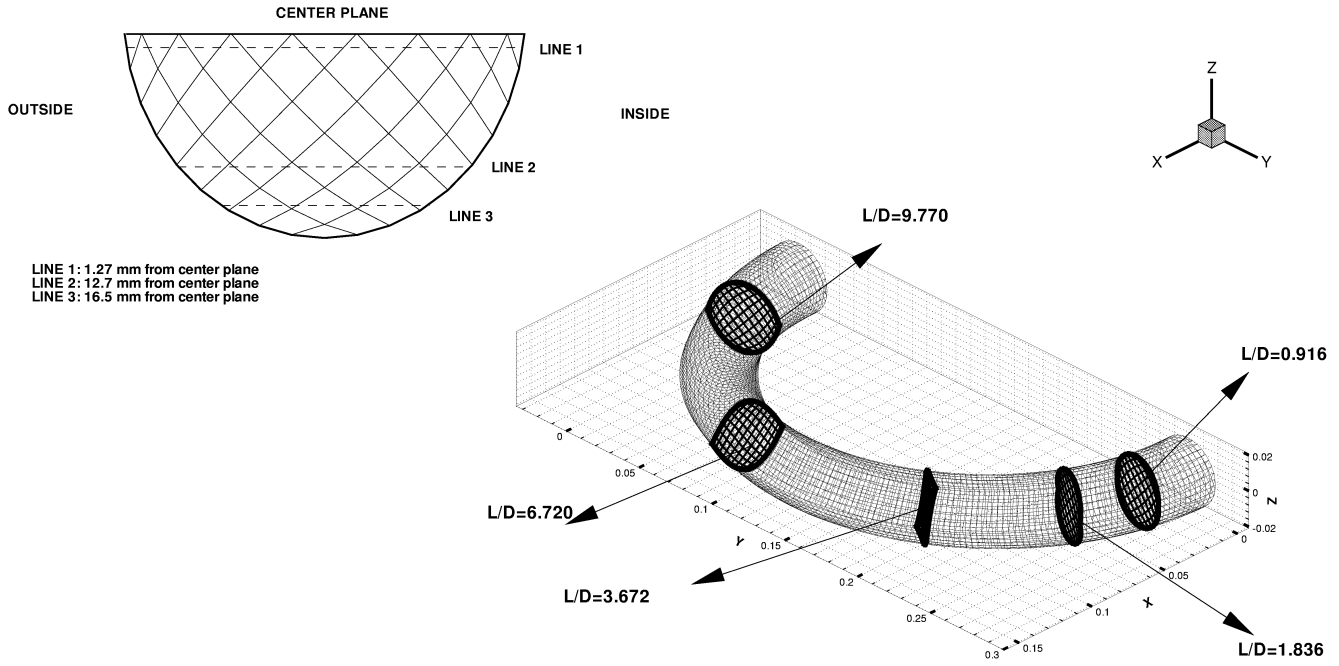

Figure 3. Curved tube simulation; inset on the upper left side shows the three cutting planes *(lines)* in the x/y plane used for validation.

2.7.3. Visualization of hemodynamical data

The resampling of the contour data for CFD purposes may result in a different number of contours or vertex points as compared to the plain surface model. As long as the restrictions outlined in Sec. 2.7.2 are satisfied, this does not have any impact on the visualization. The CFD process adds a value τ to each of the vertex points, indicating the local shear stress at that point. The τ parameter is then translated into a color, where usually green represents normal (low) shear stress, while red colors indicate high shear stresses, and blue depicts areas of reverse flow (turbulences). These colors can be easily added to the plain 3-D model described in Sec. 2.7.1 by using the `colorPerVertex` construct of the `IndexedFaceSet` node. The problem in the animated 4-D model is that the color cannot be interpolated in a similar way as demonstrated for the vertex coordinates in Sec. 2.7.2; a solution of this problem is the use of `Script` nodes to implement the additional interpolation and routing in JavaScript.

3. STUDIES

3.1. Validation

The 3-D angiographic reconstruction and the system for fusion with IVUS have been validated extensively in several phantom and in-vitro studies on cadaveric pig hearts.[20,14,16] Basis for the validation of the CFD analysis software was published data from numerous experiments performed in the 1970's at the College of Engineering, University of California at Berkeley. Their results from steady flow experiments in curved pipes using laser velocimeter techniques[23,24] were compared with the CFD analysis performed by our software on a computer simulation of an identical setup.

Since the coronary vessels have a complex curved geometry, the CFD program was initially validated for a regular curved tube geometry for which extensive experimental results have been published. We chose a curved tube model representing the radius–to–radius of curvature ratio representative of the human aortic arch for this validation study. The model consists of a tube with a diameter (D) of 3.81 cm, an axial entrance velocity of 18.1 cm/s, radius (a) to radius of curvature (R) ratio of a/R = 1/7, and a Dean no. of De=183. As shown in Fig. 3, five different cross-sections were dissected along the tube based on varying length–diameter (L/D) ratios in order to determine their velocity profiles. Symmetry was assumed in the experiments and velocity measurements were made along selected cuts which were 1.27, 12.7 and 16.5 mm away from the center plane (see Fig. 3, inset). The fluid to be simulated was

a glycerin-water mixture that approximated constant fluid property conditions of blood. The density of this mixture was ρ=1197.5 kg/m^3 while the kinematic viscosity was ν=2.8500·10^{-5} m^2/s. The details of the numerical procedure using the SIMPLEC algorithm is detailed in Lai and Przekwas.[25]

3.2. In-vivo application

3.2.1. Generation of the 4-D model

The overall fusion study currently includes seven patients undergoing routine stent placement. For the purpose of four-dimensional modeling, an in-vivo right coronary artery with a severe stenosis has been chosen for a prototypic analysis, as shown in this paper. A total of 173 heart beats have been recorded on IVUS, and the resulting frames subdivided into six different heart phases (end-diastolic, 17%, 33%, 50%, 67%, and 83% within all R–R intervals) after digitization from VHS/NTSC tape. From the angiograms, a full cycle from end-diastole to end-diastole was extracted for which optimum filling conditions with respect to the contrast dye where met. Then, six angiographic pairs were selected corresponding to the phases determined for the IVUS data. The angiograms are shown in Figure 1. For the IVUS frames, an interlacing scheme was used to assign one frame for each heart cycle to a specific heart phase, as shown in Figure 2. If a heart cycle consisted of less than six frames, one frame was assigned to two phases. In this way, all heart phases contained the same number of IVUS frames. After rectification of the angiograms for geometric image distortions, the six 3-D models have been reconstructed, where the catheter outlet and the tip of the transducer were used as landmarks. IVUS contours were downsampled to 30 radial sectors of 12° each, which results in a total of 5,160 vertex points per 3-D model. Moving average smoothing was performed along the vessel axis within each 3-D model.

3.2.2. CFD analysis of end-diastolic 3-D reconstruction

The procedure for solving flows in the 3-D coronary geometry began with smoothing the reconstructed surface using cubic splines. Next, grid generation as described in Sec. 2.6 was perfromed on the coronary vessel in the end-diastolic phase. As part of the geometry development, the grid density was optimized based on a compromise between the grid size and the structural integrity of the mesh.

The same finite-volume numerical procedure used in the curved tube for the validation as described in Sec. 3.1 was also utilized to conduct fluid flow analysis on in-vivo data. After the validation of the CFD code with flow analysis in a curved tube representative of the human aortic arch was successful, the CFD analysis was performed on the reconstructed geometry of the right coronary artery at the end-diastolic phase of the cardiac cycle. The fluid properties were specified to be representative of that of human blood based on a Reynolds number of 300. The density of blood is about $\rho = 1035\,\mathrm{kg/m^3}$ while the kinematic viscosity is about $\nu = 3.381 \cdot 10^{-6}\,\mathrm{m^2/s}$. Blood was treated as an incompressible, homogenous and Newtonian fluid. In this preliminary analysis on fluid dynamic analysis through a morphologically realistic coronary vessel geometry, we assumed the flow to be steady, with the vessel being assumed to be rigid and not translating or changing geometry with the contraction of the heart. For the inlet velocity boundary condition, a flat velocity profile under steady-state conditions was used (u≈0.52 m/s). Further, the no-slip boundary condition was specified at the vessel wall and a constant pressure outlet condition was utilized in the CFD model.

4. RESULTS AND DISCUSSION

4.1. Generation and visualization of the in-vivo 4-D model

After the complete 4-D contour data was available, the VRML scene was generated and used for visualization with a CosmoPlayer 2.1 on either SGI Onyx 2 (IRIX 6.5 operating system, 576 MB main memory) and Pentium III (NT 4.0/Win2000, 256/512 MB) machines. These configurations showed sufficient performance to view the scene, the total of 36,120 coordinate points as input for the `CoordinateInterpolator` may however hit the limits of less powerful hardware. It has to be noted that our scheme assumes a constant heart activity with approximately equally distributed R-waves. More complex acquisition schemes were developed,[19] however at the cost of substantially increased acquisition time. In this feasibility study, no effects could be recognized due to the simplifications made. The use of just six control points per contour vertex for the animation, along with the linear interpolation provided by the standard-VRML node, resulted in noticeable changes of movement direction in the visualization during the systolic part of the cycle with its rapid movement. This could be improved by replacing the standard interpolator node by a JavaScript node performing a spline-based trajectory computation.

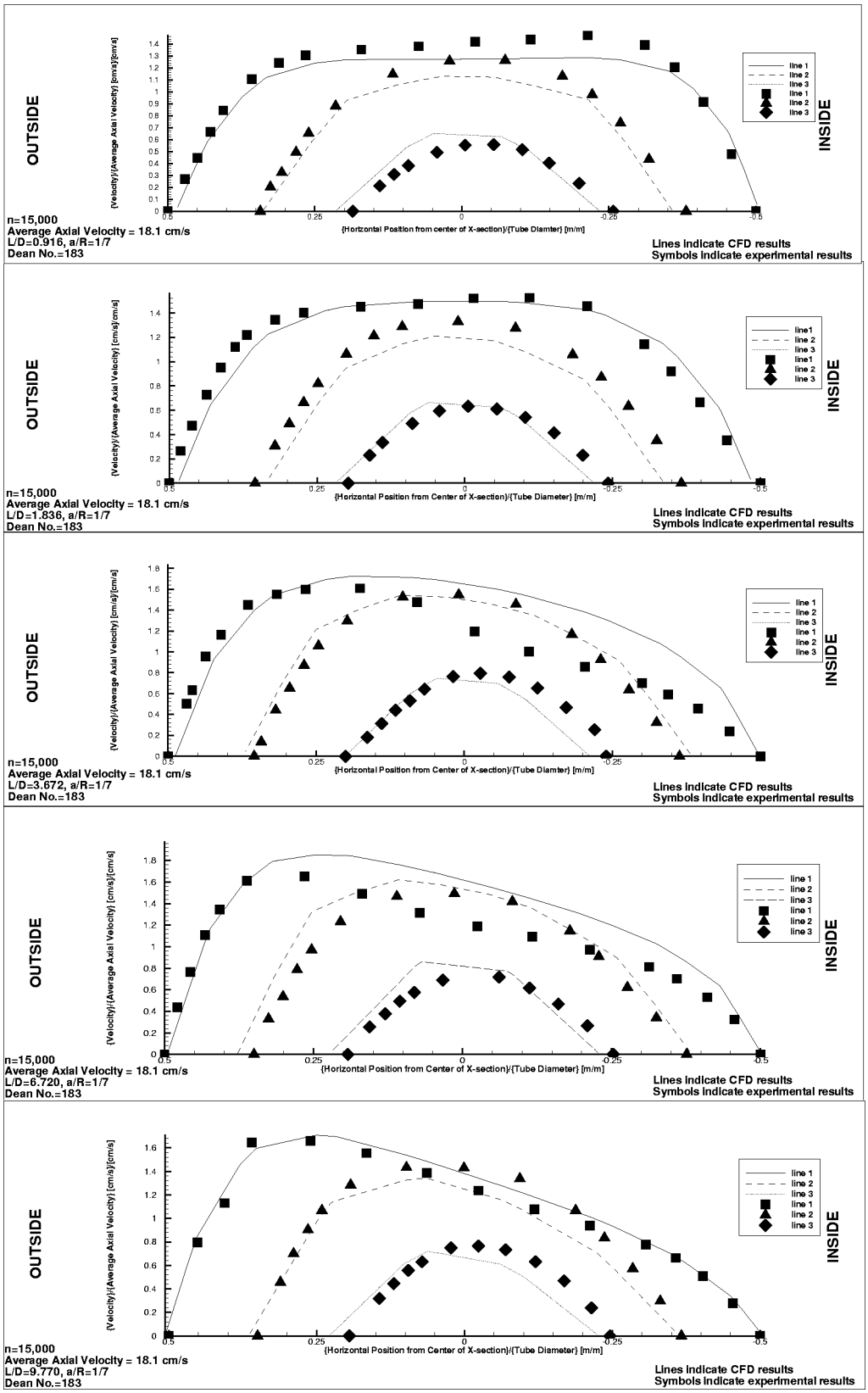

Figure 4. Results from flow physics validation of the tube shown in Figure 3.

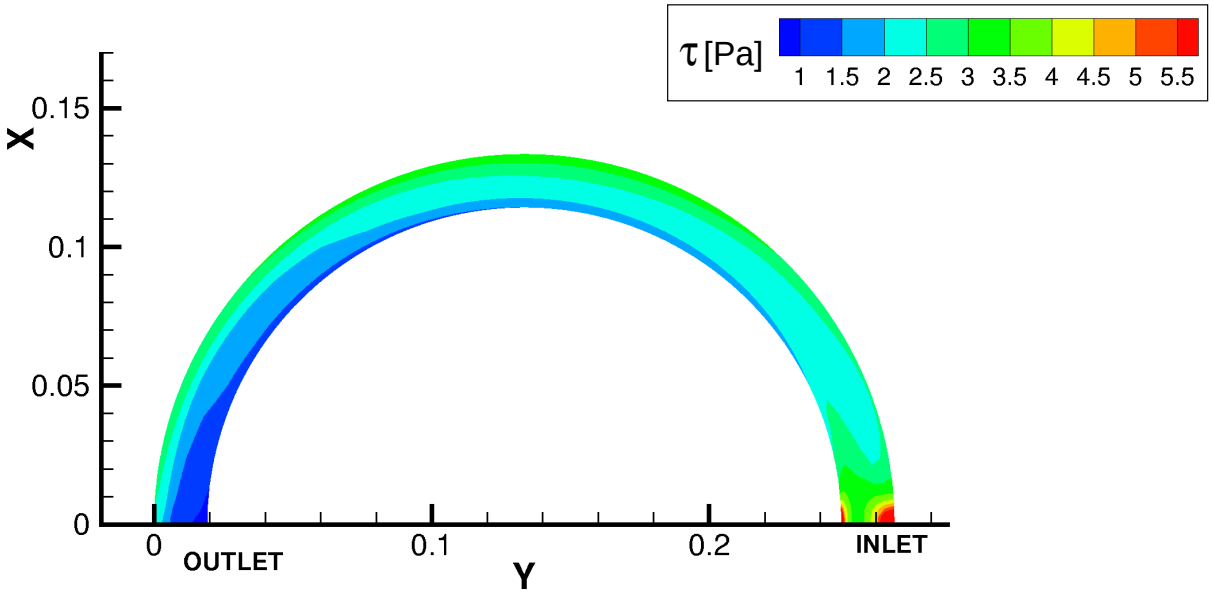

Figure 5. Shear stress distribution in tube *(this figure is available in color on the CD version or the authors' web page).*

4.2. Validation of the computational fluid dynamics analysis

4.2.1. Validation in the curved tube simulation

The computed axial velocity distribution at various cross-sections in the curved tube, represented by the axial distance (L), normalized with respect to the diameter (D) of the curved tube, are shown in Figure 4. The computed axial velocity profiles in planes parallel to the diametrical plane (as shown in Fig. 3) are compared with the corresponding experimental data plotted as symbols. A good agreement of the computed velocity profiles from the present analysis with the experimental data are evident from the figure. Due to the development of the secondary flows as the fluid traverses through the curved tube, the skewing of the axial velocity profile towards the outer wall of curvature is apparent from the plotted velocity profiles. Similar profiles have been reported by Pedley *et al.*[26] as well as Brech and Belhouse,[27] involving curvature flows at the downstream region in a biologic vessel branch.

4.2.2. Shear stress distribution in curved tube and in coronary vessel

Regions of low wall shear stresses have been implicated as sites for plaque formation in predisposed blood vessels.[28–31] Figure 5 describes the wall shear stress distribution in the x/y plane of the 3-D curved tube. Figures 6 and 7 show the results of the 3-D visualization in VRML, performed on the reconstructed in-vivo data from the right coronary artery in the end-diastolic phase, including an endoscopic view for virtual angioscopy.[18]

As seen clearly in the curve tube, the location of maximal shear stress was closer to the outer wall ($3<\tau<6$ Pa) and the minimal shear stress was closer to the inner curve ($1<\tau<3$ Pa). This is in general agreement with other CFD analysis in curved tubes and vessels.[32] The shear stress distribution in the right coronary artery, however, exhibits a complex pattern due to the complicated geometry of the vessel segment with multi-planar curvature. In addition, in the stenotic region with a significant reduction in the cross-sectional area resulting in fluid acceleration through the region of narrowing, an increased wall shear stress is observed. Distal to the narrowing, flow reversal and negative shear stresses can also be observed.

5. CONCLUSIONS

In this preliminary study, we have demonstrated the ability to reconstruct the morphologically realistic geometry of the coronary arteries from the fusion of IVUS and angiographic imaging modalities. We now have the ability of reconstruction of the coronary vessel geometry as a function of time in order to delineate the motion of the artery during a cardiac cycle. In this preliminary study, the CFD code was also validated in a curved tube geometry depicting a typical human aortic arch and comparing the results with previously published experimental results.

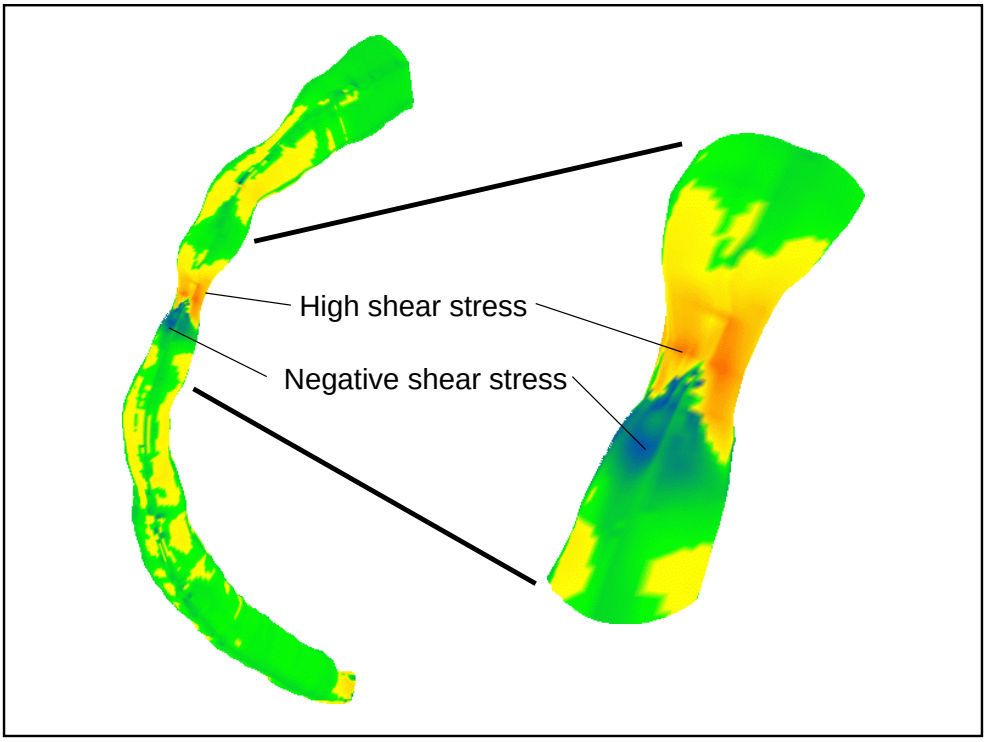

Figure 6. Result from CFD analysis, where local shear stress is color coded; note the increased shear stress proximal to the stenosis (red), while flow reversal (blue) occurs distal to the stenosis.

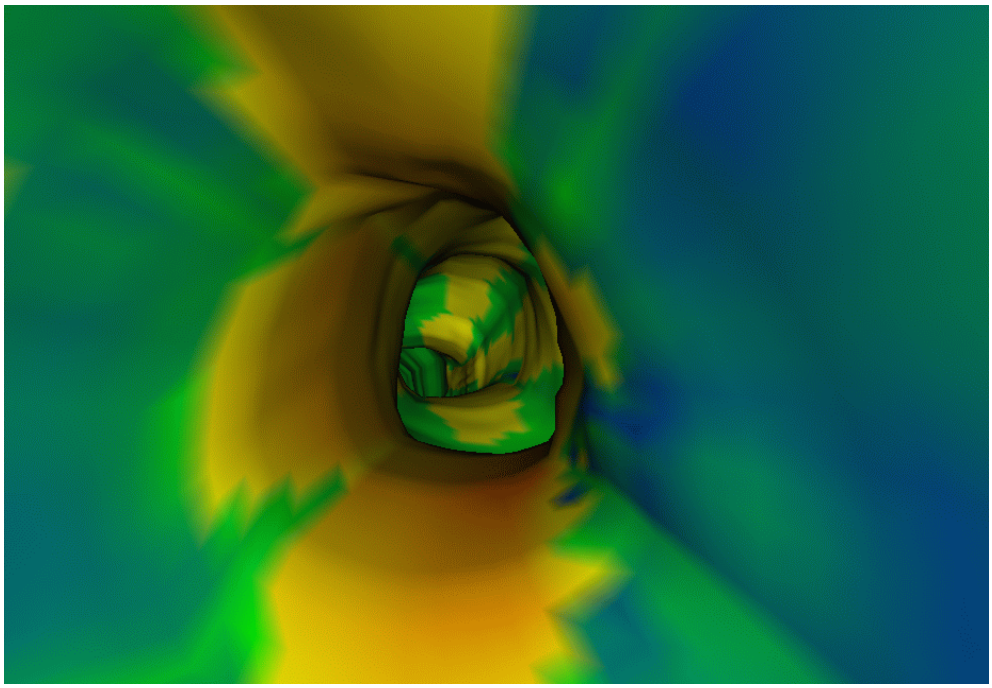

Figure 7. Endoscopic scene of the above analysis; the viewpoint is located immediately distal to the stenosis, viewing in proximal direction.

(both figures are available in color on the CD version or on the authors' web page)

Results on the shear stress distribution in a right coronary vessel at the end-diastolic phase with a stenosis has also been presented. Our aim is to use CFD simulation and the computation of wall shear stress distribution in coronary vessels with the inclusion of the vessel distensibility as well as the translation and geometrical changes of the artery during a cardiac cycle in order to correlate the flow induced stresses with the development and growth of atherosclerotic lesions in these vessels.

ACKNOWLEDGMENTS

This work is supported in part by grant 1 R01 HL63373-01 of the *National Institutes of Health* (NIH), Bethesda MD, USA; previous support was provided by grant Wa 1280/1-1 of the *Deutsche Forschungsgemeinschaft* (DFG), Bonn, Germany. The image data used within the scope of this study was acquired at the University of Iowa Hospital and Clinics, Iowa City IA, USA; the Department of Cardiology at the University Hospital of Essen, Germany; and the Brigham and Women's Hospital at Harvard Medical School, Boston MA, USA. The authors especially would like to thank Olusegun J. Ilegbusi and Zhenjun Hu, both with the Northeastern University, Boston MA, as well as Charles L. Feldman, Brigham and Women's Hospital, for their collaboration in generating the shear stress data for the visualizations shown in Figures 6 and 7.

REFERENCES

1. American Heart Association, *2001 Heart and Stroke Statistical Update*, AHA, Dallas, 2000.
2. K. B. Chandran, M. J. Vonesh, A. Roy, S. Greenfield, B. Kane, R. Greene, and D. D. McPherson, "Computation of vascular flow dynamics from intravascular ultrasound images," *Medical Engineering and Physics* **18**, pp. 295–304, June 1996.
3. A. Santamarina, E. Weydahl, J. M. Siegel, and J. E. Moore, "Computational analysis of flow in a curved tube model of the coronary arteries: Effects of time-varying curvature," *Annals of Biomedical Engineering* **26**, pp. 944–954, Nov. 1998.
4. J. L. Berry, A. Santamarina, J. E. Moore, S. Roychowdhury, and W. D. Routh, "Experimental and computational flow evaluation of coronary stents," *Annals of Biomedical Engineering* **28**, pp. 386–398, Apr. 2000.
5. K. B. Chandran, "Morphologically realistic 3D reconstruction of cardiovascular segments and hemodynamic analysis," in *Proc. 11th International Conference on Mechanics in Medicine and Biology, Maui HI*, pp. 161–162, ICMMB, 2000.
6. R. M. Nerem and W. A. Seed, "Coronary artery geometry and its fluid-mechanical implications," in *Fluid Dynamics as a Localizing Factor for Atherosclerosis*, G. Schettler, R. M. Nerem, H. Schmid-Schönbein, H. Mörl, and C. Diehm, eds., pp. 51–59, Springer, (Berlin/New York), 1982/83.
7. S. L. Waters, "Coronary artery haemodynamics: Pulsatile flow in a tube of time-dependent curvature." Ph.D. Thesis, University of Leeds, United Kingdom, 1996.
8. R. L. Kirkeeide, P. Fung, R. W. Smalling, and K. L. Gould, "Automated evaluation of vessel diameter from arteriograms," in *Proc. Computers in Cardiology 1982, Seattle WA*, pp. 215–218, IEEE-CS Press, (Los Alamitos CA), 1982.
9. J. Beier, H. Oswald, H. U. Sauer, and E. Fleck, "Accuracy of measurement in quantitative coronary angiography (QCA)," in *Computer Assisted Radiology (CAR '91)*, H. U. Lemke, M. L. Rhodes, C. C. Jaffe, and R. Felix, eds., pp. 721–726, Springer, (Berlin/New York), 1991.
10. J. H. C. Reiber, G. Koning, J. Dijkstra, A. Wahle, B. Goedhart, F. H. Sheehan, and M. Sonka, "Angiography and intravascular ultrasound," in *Handbook of Medical Imaging — Volume 2: Medical Image Processing and Analysis*, M. Sonka and J. M. Fitzpatrick, eds., pp. 711–808, SPIE Press, (Bellingham WA), 2000.
11. M. Sonka, X. Zhang, M. Siebes, M. S. Bissing, S. C. DeJong, S. M. Collins, and C. R. McKay, "Segmentation of intravascular ultrasound images: A knowledge-based approach," *IEEE Transactions on Medical Imaging* **14**, pp. 719–732, Dec. 1995.
12. X. Zhang, C. R. McKay, and M. Sonka, "Tissue characterization in intravascular ultrasound images," *IEEE Transactions on Medical Imaging* **17**, pp. 889–899, Dec. 1998.
13. A. Wahle, G. P. M. Prause, C. von Birgelen, R. Erbel, and M. Sonka, "Automated calculation of the axial orientation of intravascular ultrasound images by fusion with biplane angiography," in *Medical Imaging 1999: Image Processing*, K. M. Hanson, ed., vol. 3661, pp. 1094–1104, SPIE Proceedings, (Bellingham WA), 1999.

14. A. Wahle, G. P. M. Prause, S. C. DeJong, and M. Sonka, "Geometrically correct 3-D reconstruction of intravascular ultrasound images by fusion with biplane angiography — methods and validation," *IEEE Transactions on Medical Imaging* **18**, pp. 686–699, Aug. 1999.
15. A. Wahle, G. P. M. Prause, C. von Birgelen, R. Erbel, and M. Sonka, "Fusion of angiography and intravascular ultrasound in-vivo: Establishing the absolute 3-D frame orientation," *IEEE Transactions on Biomedical Engineering — Biomedical Data Fusion* **46**, pp. 1176–1180, Oct. 1999.
16. A. Wahle, S. C. Mitchell, M. E. Olszewski, R. M. Long, and M. Sonka, "Accurate visualization and quantification of coronary vasculature by 3-D/4-D fusion from biplane angiography and intravascular ultrasound," in *European Biomedical Optics Week (EBiOS 2000): Biomonitoring and Endoscopy Technologies*, I. Gannot, Y. V. Gulyaev, T. G. Papazoglou, and C. F. P. van Swol, eds., vol. 4158, pp. 144–155, SPIE Europto, (Bellingham WA), 2000/2001.
17. A. L. Ames, D. R. Nadeau, and J. L. Moreland, *The VRML 2.0 Sourcebook*, John Wiley and Sons, New York, 2nd ed., 1997.
18. A. Wahle, S. C. Mitchell, S. D. Ramaswamy, K. B. Chandran, and M. Sonka, "Virtual angioscopy in human coronary arteries with visualization of computational hemodynamics," in *Medical Imaging 2001: Physiology and Function from Multidimensional Images*, C. Chen and A. V. Clough, eds., vol. 4321, SPIE Proceedings, (Bellingham WA), Feb. 2001.
19. N. Bruining, C. von Birgelen, M. T. Mallus, P. J. de Feyter, E. de Vrey, W. Li, F. Prati, P. W. Serruys, and J. R. T. C. Roelandt, "ECG-gated ICUS image acquisition combined with a semi-automated contour detection provides accurate analysis of vessel dimensions," in *Proc. Computers in Cardiology 1996, Indianapolis IN*, pp. 53–56, IEEE Press, (Piscataway NJ), 1996.
20. A. Wahle, E. Wellnhofer, I. Mugaragu, H. U. Sauer, H. Oswald, and E. Fleck, "Assessment of diffuse coronary artery disease by quantitative analysis of coronary morphology based upon 3-D reconstruction from biplane angiograms," *IEEE Transactions on Medical Imaging* **14**, pp. 230–241, June 1995.
21. M. Sonka, V. Hlavac, and R. Boyle, *Image Processing, Analysis, and Machine Vision*, PWS Publishing, Pacific Grove, 2nd ed., 1998/99.
22. C. H. Zeng and M. Sonka, "Local three-dimensional shape-preserving smoothing without shrinkage," in *Proc. ICIP '97, International Conference on Image Processing*, vol. 1, pp. 393–396, IEEE Press, (Piscataway NJ), 1997.
23. Y. C. Agrawal, "Laser velocimeter study of entrance flows in curved pipes." Ph.D. Thesis, University of California at Berkeley, United States, 1975.
24. Y. C. Agrawal, L. Talbot, and K. Gong, "Laser anemometer study of flow development in curved circular pipes," *Journal of Fluid Mechanics* **85**(3), pp. 497–518, 1978.
25. Y. G. Lai and A. J. Przekwas, "A finite-volume method for fluid flow simulations with moving boundaries," *Computational Fluid Dynamics* **2**, pp. 19–40, 1994.
26. T. J. Pedley, R. C. Schroter, and M. F. Sudlow, "Flow and pressure drop in systems of repeatedly branching tubes," *Journal of Fluid Mechanics* **46**(2), pp. 365–383, 1971.
27. R. Brech and B. J. Bellhouse, "Flow in branching vessels," *Cardiovascular Research* **7**, pp. 593–600, Sept. 1973.
28. K. B. Chandran, *Cardiovascular Biomechanics*, New York University Press, New York/London, 1992.
29. M. H. Friedman, C. B. Bargeron, O. J. Deters, G. M. Hutchins, and F. F. Mark, "Correlation between wall shear and intimal thickness at a coronary artery branch," *Atherosclerosis* **68**, pp. 27–33, Nov. 1987.
30. M. H. Friedman, C. B. Bargeron, D. D. Duncan, G. M. Hutchins, and F. F. Mark, "Effects of arterial compliance and non-newtonian rheology on correlations between intimal thickness and wall shear," *Journal of Biomechanical Engineering* **114**, pp. 317–320, Aug. 1992.
31. C. M. Gibson, L. Diaz, K. Kandarpa, F. M. Sacks, R. C. Pasternak, T. Sandor, C. L. Feldman, and P. H. Stone, "Relation of vessel wall shear stress to atherosclerosis progression in human coronary arteries," *Arteriosclerosis and Thrombosis* **13**, pp. 310–315, Feb. 1993.
32. R. Krams, J. J. Wentzel, J. A. F. Oomen, R. Vinke, J. C. H. Schuurbiers, P. J. de Feyter, P. W. Serruys, and C. J. Slager, "Evaluation of endothelial shear stress and 3-D geometry as factors determining the development of atherosclerosis and remodeling in human coronary arteries in-vivo; combining 3-D reconstruction from angiography and IVUS (ANGUS) with computational fluid dynamics," *Arteriosclerosis, Thrombosis and Vascular Biology* **17**, pp. 2061–2065, Oct. 1997.